Available online at www.sciencedirect.com
SCIENCE DIRECT
Trans. Nonferrous Met. Soc. China 16(2006) 502−506
Transactions of Nonferrous Metals Society of China
www.csu.edu.cn/ysxb/

# Microstructure and high-temperature shape-memory effect in $Ni_{54}Mn_{25}Ga_{21}$ alloy

MA Yun-qing(马云庆)[1], JIANG Cheng-bao(蒋成保)[2], LI Yan(李 岩)[2],
XU Hui-bin(徐惠彬)[2], WANG Cui-ping(王翠萍)[1], LIU Xing-jun(刘兴军)[1]

1.Department of Materials Science and Engineering, Xiamen University, Xiamen 361005, China;
2.Department of Materials Science and Engineering, Beijing University of Aeronautics and Astronautics, Beijing 100083, China

Received 25 August 2005; accepted 10 March 2006

**Abstract:** $Ni_{54}Mn_{25}Ga_{21}$ alloy was prepared to investigate the microstructure, martensitic transformation and high-temperature shape-memory effect. $Ni_{54}Mn_{25}Ga_{21}$ alloy exhibits single phase of non-modulated martensite with tetragonal structure at room temperature. Its martensitic start temperature $M_s$, martensitic finish temperature $M_f$ on cooling, and austenitic start temperature $A_s$, austenitic finish temperature $A_f$ on heating are 260.2, 237.8, 262.5 and 287.8 ℃, respectively. The compressive strength and strain of $Ni_{54}Mn_{25}Ga_{21}$ single crystal were measured to be 845 MPa and 20.5%, respectively, with compressive axis along the growth direction of the rods. An excellent shape-memory strain of 6.1%, which is the best performance among high-temperature shape-memory alloys up to the present, is obtained when prestrained to 8%.

**Key words:** $Ni_2MnGa$ Heusler alloy; microstructure; martensitic transformation; high-temperature shape-memory effect

## 1 Introduction

Shape memory alloys (SMAs) have developed rapidly in the past few decades as new functional materials, with commercial applications in pipe couplings, medical implants, electrical connectors and various actuators etc[1−3]. But the highest operation temperature is limited to about 100 ℃ due to the low martensitic transformation temperatures or the poor thermal stability of TiNi, CuZnAl and CuAlNi, which are the three commercially important SMAs[1,2]. However, many engineering cases need SMAs to function at high temperatures (i.e. higher than 200 ℃), such as in aerospace and automotive engines. There is a pressing need to develop high-temperature shape-memory alloys (HTSMAs), and several alloy systems have been investigated, such as Cu-based alloys, NiAl, TiNi(Hf, Zr) and TiNiPd[4−10], but till now some problems still remain unsolved in these alloys. For instance, Cu-based and NiAl HTSMAs are considered unstable because equilibrium phases, which are detrimental to the shape-memory effect (SME), precipitate at high temperatures[4−6]. NiTiZr and NiTiHf HTSMAs are too brittle for practical use[7]. As regards the NiTiPd alloy, although its full recovery strain has been increased to 5.5% by proper thermomechanical treatment[8], the high cost of precious metal Pd hinders its potential application. The studies to explore low-cost HTSMAs keep active.

Recently, $Ni_2MnGa$ Heusler alloys, which possess a bcc $L2_1$ structure at high temperature and undergo a martensitic transformation to a complex tetragonal structure upon cooling, have been extensively explored as ferromagnetic SMAs[11−13]. Several papers reported that high martensitic transformation temperatures (up to 350 ℃) exist in NiMnGa alloys with Ni or Mn content higher than the stoichiometric $Ni_2MnGa$, showing their potentials as HTSMA[14−17]. In this study, the microstructure, martensitic transformation behaviors as well as high-temperature SMEs of $Ni_{54}Mn_{25}Ga_{21}$ alloy were studied, which will be beneficial for the development of the alloys as HTSMA.

## 2 Experimental

Polycrystalline ingots of $Ni_{54}Mn_{25}Ga_{21}$ alloy were

**Foundation item:** Project(50371005) supported by the National Natural Science Foundation of China
**Corresponding author:** MA Yun-qing; Tel: +86-592-2189688; E-mail: myq@xmu.edu.cn

remelted four times by the arc melter with high purity element (99.9%) under argon atmosphere. The mass loss was found to be less than 0.2%. Homogenization was performed by sealing the ingots under vacuum in quartz ampoules and annealing at 900 ℃ for 72 h, followed by the water quench.

The X-ray diffraction analysis was performed by a Regaku D/Max 2200 PC diffractometer equipped with a heating stage. A Cu $K_\alpha$ radiation was used in the experiments. The microstructure was observed by optical microscope and TEM (Hitachi H-800 operating at 200 kV). Specimens for optical observation were mechanically polished and etched in a solution of 99 mL methanol+2 mL nitric acid+5 g ferric chloride. Thin foils for TEM observation were got from specimens by sparking method. They were first mechanically ground to about 80 μm thick, and then electropolished using twin-jet method in an electrolyte of 10% perchloric acid + 90% acetic acid. The forward and reverse martensitic transformation temperatures were determined by differential scanning calorimetry(DSC) modeled NETZSCH STA449 with the cooling and heating rate of 10 ℃/min.

The SMEs of $Ni_{54}Mn_{25}Ga_{21}$ alloys were performed using single crystals, which were prepared by zone-melting unidirectional solidification. Master rods with the diameter of 7.2 mm and the length of 110 mm were obtained by drop casting equipment attached to the arc melter. Then master rods were used to prepare single crystals by zone-melting unidirectional solidification in XLL 500 furnace with the pulling rate of 10 mm/h. The furnace chamber was first vacuumed to $2\times10^{-3}$ Pa, followed by backfilling high purity argon gas to $0.5\times10^5$ Pa.

Single crystal specimens of 3 mm×3 mm×5 mm size for uniaxial compression were cut from the as-grown rods with the long edge parallel to the pulling direction. The uniaxial compression experiments were carried out at room temperature on the MTS-880 materials testing system with the compression direction parallel to the long edge of the specimens. The speed of the crosshead was 0.05 mm/min, corresponding to an initial strain rate of $1.6\times10^{-4}$ $s^{-1}$. The heights of the specimens were measured before loading ($l_0$), after loading ($l_1$) and after heating to 400 ℃ for 10 min ($l_2$) by a micrometer with an accuracy of 0.01 mm. The pre-strain during compression was defined as $\varepsilon_{pre}=\Delta l/l_0$, where $\Delta l$ is the displacement of the crosshead. The residual strain after unloading ($\varepsilon_r$), permanent strain ($\varepsilon_p$) and strain which recovered due to the SME ($\varepsilon_{SME}$) were obtained as: $(l_1-l_0)/l_0\times100\%$, $(l_2-l_0)/l_0\times100\%$ and $(l_1-l_2)/l_1\times100\%$, respectively. The recovery rate($R$) was calculated as $R=\varepsilon_{SME}/(\varepsilon_{SME}+\varepsilon_p)\times100\%$.

## 3 Results and discussion

### 3.1 Microstructure and martensitic transformation

The powder X-ray diffraction pattern at room temperature, which is shown in Fig.1, indicates that $Ni_{54}Mn_{25}Ga_{21}$ alloy possesses pure martensitic structure. All the reflections can be indexed by the complex tetragonal structure with $a=b$=0.767 1 nm, $c$=0.668 9 nm and $c/a$=0.872. The lattice parameters are different from those of low-temperature martensite in stoichiometric $Ni_2MnGa$ alloy[18]. The partial substitution of Ni for Ga leads to the shrinkage of unit-cell volume and the increase of electronic concentration, which are considered to induce the distortion of the $L2_1$ cubic structure, resulting in the increase of martensitic transformation temperature and the appearance of the martensitic structure at room temperature. This agrees well with the previous results that NiMnGa alloys with higher Ni content than stoichiometric $Ni_2MnGa$ exhibit non-modulated martensite[13, 18].

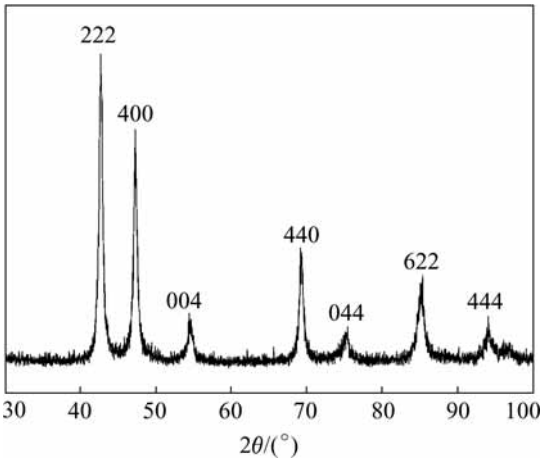


**Fig.1** Powder XRD pattern of polycrystal $Ni_{54}Mn_{25}Ga_{21}$ alloy at room temperature

Fig.2 shows the optical morphology of $Ni_{54}Mn_{25}Ga_{21}$ alloy at room temperature. Lamellar twin variants exist in every grain, and exhibit the configurations of typical self-accommodation arrangement. The interfaces among twin variants are straight and clear, exhibiting good characteristics of thermoelasticity. Fig.3 shows the TEM images and the selected area electron diffraction(SAED) patterns of $Ni_{54}Mn_{25}Ga_{21}$ alloy. The typical bright field image exhibits a stripe-like morphology with well-accommodated martensite plates (Fig.3(a)). The martensite is confirmed to be a tetragonal structure, which is identical with the X-ray diffraction results. The SAED pattern shown in Fig.3(b) was taken from the boundary of each big martensitic plate (area marked with $A$ in Fig.3(a)) and indexed to be the twins

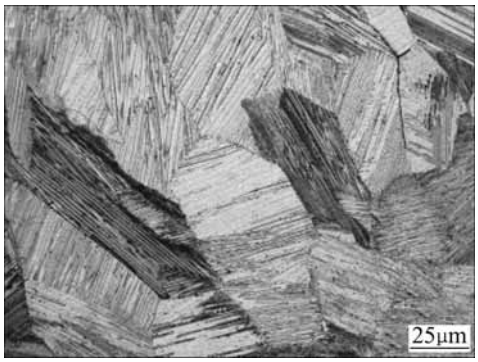


**Fig.2** Optical observation of $Ni_{54}Mn_{25}Ga_{21}$ alloy at room temperature

along (111) planes. The twin structure of each big martensitic plate is also confirmed by Figs.3(c) and (d), which are the central dark field images taken from the reflection spots of $22\bar{2}_M$ and $\bar{2}\,\bar{2}2_T$ indicated in Fig.3(b), respectively. Micrographs of smaller stripes arranged in regular direction exist inside each big martensitic plate, as shown in area *B* marked in Fig.3(a). The SAED pattern taken from this area also exhibits (111) twins, which is shown in Fig.3(e) when the incident electron beam is tilted to $[01\bar{1}]$. In general, the microstructure of $Ni_{54}Mn_{25}Ga_{21}$ alloy consists of coarse twins on the order of 1 μm to 5 μm in width with an internal structure of fine twins about 0.05 μm to 0.1 μm in width, which are both twinned along the {111} plane. The strict twin structure of the microstructure is beneficial to the thermoelasticity of its martensitic transformation.

The DSC measurements were performed for the $Ni_{54}Mn_{25}Ga_{21}$ alloy, and the results are shown in Fig.4. It can be seen that there is only one endothermic or exothermic peak in the heating or cooling DSC curves, respectively, indicating that one phase transformation appear in each run. The martensitic transformation temperatures were determined by the tangent method

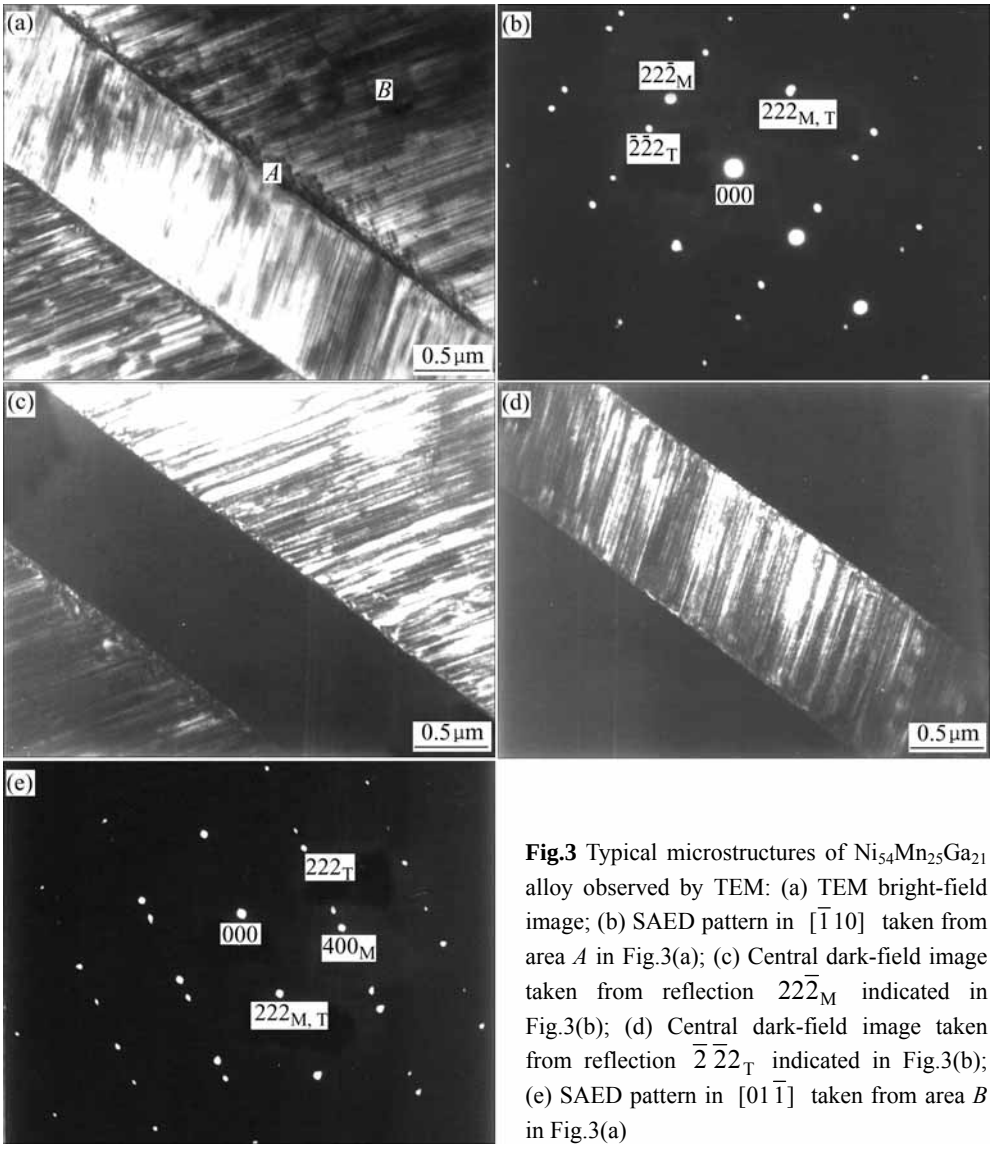


**Fig.3** Typical microstructures of $Ni_{54}Mn_{25}Ga_{21}$ alloy observed by TEM: (a) TEM bright-field image; (b) SAED pattern in $[\bar{1}10]$ taken from area *A* in Fig.3(a); (c) Central dark-field image taken from reflection $22\bar{2}_M$ indicated in Fig.3(b); (d) Central dark-field image taken from reflection $\bar{2}\,\bar{2}2_T$ indicated in Fig.3(b); (e) SAED pattern in $[01\bar{1}]$ taken from area *B* in Fig.3(a)

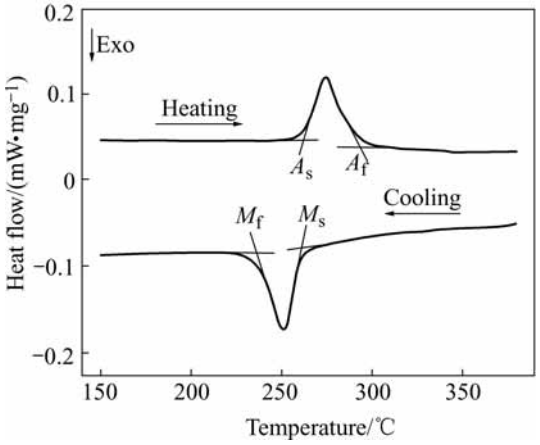


**Fig.4** DSC curves of $Ni_{54}Mn_{25}Ga_{21}$ alloy showing forward (on cooling) and reverse (on heating) martensitic transformations

from the DSC curves. The martensitic start temperature $M_s$, martensitic finish temperature $M_f$ on cooling, and the austenitic start temperature $A_s$, austenitic finish temperature $A_f$ on heating are 260.2, 237.8, 262.5 and 287.8 ℃, respectively.

### 3.2. High-temperature shape-memory effect

Fig.5 shows the compression curve of $Ni_{54}Mn_{25}Ga_{21}$ single crystal at room temperature. The symbol (×) represents the fracture point. The compressive strength and the strain were measured to be 845 MPa and 20.5%, respectively. Its compression curve consists of three obvious stages: 1) at the beginning of the deformation, a monotonic increase in the stress with increasing strain, 2) a stress-plateau with increasing strain, and 3) a further increase in the stress with increasing deformation leading to break. The three stages are associated with the elastic deformation of the multi-variants, reorientation of martensitic variants and/or detwinning, and the elastic and plastic deformation of fully reoriented martensites, respectively[19,20]. The stress—strain curve of $Ni_{54}Mn_{25}Ga_{21}$ exhibits a stress-plateau, resulted from the reorientation of martensitic variants, which is different from other HTSMAs such as TiNiHf[21], and TiNiPd[8], where the stress-plateau completely disappears and high work harding is constantly observed, due to the dislocation slip during the reorientation of martensitic variants. It is well known that the strain recovering due to SME occurs solely through the motion of the intervariant boundaries, without any contribution from normal slip. From this point, $Ni_{54}Mn_{25}Ga_{21}$ will exhibit better SME than TiNiHf or TiNiPd alloys.

Table 1 summarizes the shape-memory behaviors of $Ni_{54}Mn_{25}Ga_{21}$ at different pre-strains. It can be seen that the complete recovery is obtained for not more than 6% prestrains, the maximum SME of 6.1% is obtained for 8% prestrain, and the SME degrade for further prestrained to 10%. This maximum SME of 6.1% is the highest one among present HTSMAs, compared with 3% for TiNiHf[21] and 5.5% for TiNiPd[8]. The high critical stress for reorientation of martensitic variants and high work hardening are thought to be responsible for their inferior SME to $Ni_{54}Mn_{25}Ga_{21}$.

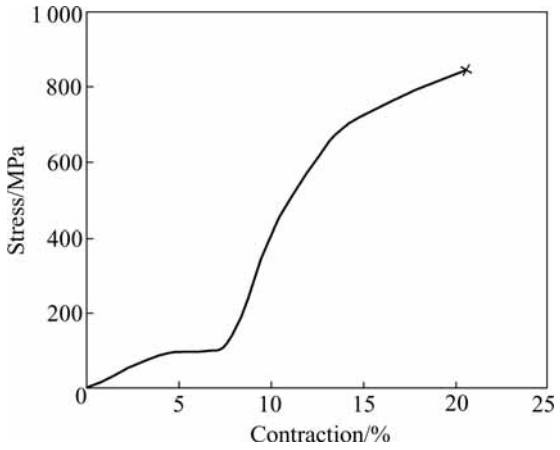


**Fig.5** Compression curve along growth direction of $Ni_{54}Mn_{25}Ga_{21}$ single crystal at room temperature

**Table 1** Shape-memory behavior of $Ni_{54}Mn_{25}Ga_{21}$ at different pre-strains

| Pre-strain, $\varepsilon_{pre}$/% | Strain after unloading, $\varepsilon_r$/% | Strain after heating, $\varepsilon_p$/% | SME strain, $\varepsilon_{SME}$/% | Recovery ratio, $R$/% |
|---|---|---|---|---|
| 4 | 3.4 | 0 | 3.4 | 100 |
| 6 | 5.2 | 0 | 5.2 | 100 |
| 8 | 6.5 | 0.4 | 6.1 | 93.8 |
| 10 | 7.7 | 1.7 | 6.0 | 77.9 |

## 4 Conclusions

1) $Ni_{54}Mn_{25}Ga_{21}$ alloy exhibits single phase of non-modulated martensite with tetragonal structure of $a=b$=0.767 1 nm, $c$=0.668 9 nm and $c/a$=0.872.

2) The microstructure analysis indicates that $Ni_{54}Mn_{25}Ga_{21}$ alloy exhibits good self-accommodation configuration with the characteristic of coarse twins width of 1−5 μm, and these coarse twins consist of inner fine micro-twins with the width of 0.05−0.1 μm, which are both twinned along the {111} plane. The strictly twinned microstructure is beneficial to the thermo-elasticity of its martensitic transformation.

3) The martensitic start temperature $M_s$, martensitic finish temperature $M_f$ on cooling, and the austenitic start temperature $A_s$, austenitic finish temperature $A_f$ on heating of $Ni_{54}Mn_{25}Ga_{21}$ alloy are 260.2, 237.8, 262.5 and 287.8 ℃, respectively.

4) The compressive strength and strain of $Ni_{54}Mn_{25}Ga_{21}$ single crystal were measured to be 845 MPa and 20.5%, respectively, with compressive axis along the growth direction of the rods at room

temperature. An excellent SME of 6.1%, which is the best performance among HTSMAs up to the present, is obtained when prestrained to 8%.

## References


[1] OTSUKA K, REN X B. Recent developments in the research of shape memory alloys[J]. Intermetallics, 1999, 7: 511−528.

[2] OTSUKA K, WAYMAN C M. Shape Memory Materials[M]. Cambridge: Cambridge University Press, 1998.

[3] SUTOU Y, OMORI T, WANG J J, et al. Characteristics of Cu-Al-Mn-based shape memory alloys and their applications[J]. Mater Sci Eng, 2004, 378: 278−282.

[4] MA Yun-qing, JIANG Cheng-bao, XU Hui-bin. Martensitic transformation and thermal stability in Cu-Al-Co and Cu-Al-Zr alloys[J]. Acta Metall Sinica, 2003, 16(6): 445−448.

[5] GEORGE E P, LIU C T, HORTON J A, et al. Characterization, processing and alloy design of NiAl-based shape memory alloys[J]. Mater Character, 1997, 39: 665−686.

[6] MA Yun-qing, JIANG Cheng-bao, DENG Li-fen, et al. Effects of composition and thermal cycle on transformation behaviors, thermal stability and mechanical properties of CuAlAg alloys[J]. J Mater Sci Tech, 2003, 19(5): 431−434.

[7] HSIEH S F, WU S K. A study on ternary Ti-rich TiNiZr shape memory alloys[J]. Mater Character, 1998, 41: 151−162.

[8] GOLBERG D, XU Y, MURAKAMI Y, et al. Improvement of a $Ti_{50}Pd_{30}Ni_{20}$ high temperature shape memory alloy by thermomechanical treatments[J]. Scripta Metall Mater, 1994, 30: 1349−1354.

[9] HUMBEECK J V. High temperature shape memory alloys[J]. J Eng Mater Tech, 1999, 121: 98−101.

[10] XU Y, SHIMIZU S, SUZUKI Y, et al. Recovery and recrystallization processes in Ti-Pd-Ni high-temperature shape memory alloys[J]. Acta Mater, 1997, 45: 1503−1511.

[11] ULLAKKO K, HUANG J K, KANTNER C, et al. Large magnetic-field-induced strains in $Ni_2MnGa$ single crystals [J]. Appl Phys Lett, 1996, 69: 1966−1968.

[12] JIANG Cheng-bao, FENG Gen, XU Hui-bin. Co-occurrence of magnetic and structural transitions in the Heusler alloy $Ni_{53}Mn_{25}Ga_{22}$ [J]. Appl Phys Lett, 2002, 80: 1619−1621.

[13] PONS J, CHERNENKO V A, SANTAMARTA R, et al. Crystal structure of martensitic phases in Ni-Mn-Ga shape memory alloys [J]. Acta Mater, 2000, 48: 3027−3038.

[14] CHERNENKO V A, CESARI E, KOKORIN V V, et al. The development of new ferromagnetic shape memory alloys in Ni-Mn-Ga system [J]. Scripta Metall Mater, 1995, 33: 1239−1244.

[15] XU Hui-bin, MA Yun-qing, JIANG Cheng-bao. A high-temperature shape-memory alloy $Ni_{54}Mn_{25}Ga_{21}$ [J]. Appl Phys Lett, 2003, 82: 3206−3208.

[16] JIN X, MARIONI M, BONO D, et al. Empirical mapping of Ni-Mn-Ga properties with composition and valence electron concentration [J]. J Appl Phys, 2002, 91: 8222−8224.

[17] MA Yun-qing, JIANG Cheng-bao, FENG Gen, et al. Thermal stability of the $Ni_{54}Mn_{25}Ga_{21}$ Heusler alloy with high temperature transformation [J]. Scripta Mater, 2003, 48: 365−369.

[18] WEDEL B, SUZUKI M, MURAKAMI Y, et al. Low temperature crystal structure of Ni-Mn-Ga alloys [J]. J Alloys Comp, 1999, 290: 137−143.

[19] GALL K, SEHITOGLU H, CHUMLYAKOV Y I, et al. Tension-compression asymmetry of the stress–strain response in aged single crystal and polycrystalline NiTi [J]. Acta Mater, 1999, 47: 1203−1217.

[20] LIU Y, XIE Z, HUMBEECK J V, et al. Asymmetry of stress–strain curves under tension and compression for NiTi shape memory alloys [J]. Acta Mater, 1998, 46: 4325−4338.

[21] MENG Xiang-long, ZHENG Yu-feng, WANG Z, et al. Shape memory properties of the $Ti_{36}Ni_{49}Hf_{15}$ high temperature shape memory alloy [J]. Mater Letters, 2000, 45: 128−132.


**(Edited by YUAN Sai-qian)**